THE JOURNAL OF PHYSICAL CHEMISTRY A

Article

pubs.acs.org/JPCA

Terahertz Spectroscopy of the Explosive Taggant 2,3-Dimethyl-2,3-Dinitrobutane

Ewelina M. Witko and Timothy M. Korter*

Department of Chemistry, Syracuse University, 1-014 Center for Science and Technology, Syracuse, New York 13244, United States

Supporting Information

ABSTRACT: The terahertz spectrum of the crystalline explosive taggant 2,3-dimethyl-2,3-dinitrobutane ($C_6H_{12}N_2O_4$) has been investigated as an alternative means of detecting solid-state explosives. The room-temperature spectrum exhibits two broad absorption features centered at 38.3 and 49.2 cm^{-1}. Once the sample is cooled to liquid-nitrogen temperatures, the resolution of three additional peaks occurs, with absorption maxima now appearing at 40.1, 47.5, 56.6, 63.9, and 73.6 cm^{-1}. Solid-state density functional theory simulations, both with and without London force dispersion corrections, have been used for the assignment of the experimental cryogenic THz spectrum to specific molecular motions in the crystalline solid. The B3LYP hybrid density functional paired with the 6-311G(2d,2p) basis set provides an excellent reproduction of the experimental data revealing that the THz spectrum arises from a mixture of intramolecular torsional vibrations localized primarily in the nitro groups and intermolecular lattice vibrations composed of rigid molecular rotations.

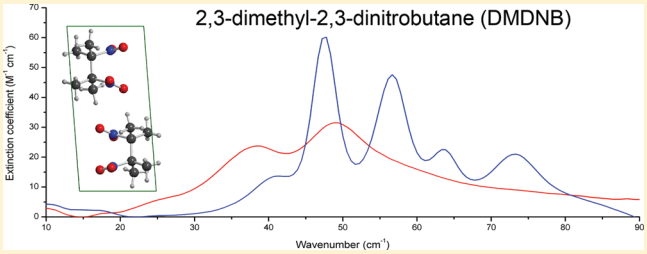

1. INTRODUCTION

Terahertz (THz) spectroscopy has proven to be a useful technique in the detection and identification of various types of explosives, from military-grade to homemade explosives to explosives-related compounds.[1−3] It is particularly attractive in this application since THz radiation (far-infrared, ∼4 to 400 cm^{-1}) can easily penetrate many common fabrics, plastics, and papers, while at the same time being nonionizing and safe for the personnel involved with the measurements.[4] Terahertz spectroscopy provides chemical information by probing low-frequency lattice vibrations (optical translations and rotations) of crystalline solids, which are sensitive to both molecular identity and also to the packing arrangement of the molecules in the solid-state.[5,6] This sensitivity of THz spectroscopy to crystal structure results in THz spectra being specific to the assayed compounds (including different polymorphs of the same compound[7]) and allows the data to be used as a fingerprint for identification of the substance. However, given the nature of the types of vibrations existing in the THz region, spectral interpretation is more challenging than in the mid-infrared. Since there are no characteristic functional group frequencies to aid in the interpretation of THz spectra of molecular solids, computational methods utilizing solid-state techniques must be employed to allow for assignment of the observed absorption features.[8−12]

While many solid-state explosives exhibit distinct THz spectra, not all do,[13] and therefore, it is possible that the substance may alternatively be detected and identified through the THz absorption of an added taggant molecule. Since the early 1990s, two laws, the Antiterrorism Act of 1996 in the United States and another by the International Civil Aviation Organization in 1991, have been passed that require the addition of detecting taggants to plastic bonded explosives (i.e., PETN and HMX) and, consequently, making it illegal to manufacture, sell, and import these explosives without any detection agent.[14,15] Generally, the taggant agent cannot alter the properties of the tagged explosive as well as having a much higher vapor pressure than the explosive itself, which consequently allows for easier detection of the concealed explosive[16] using techniques such as ion-mobility spectrometry. Commonly used taggants include 2-nitrotoluene, 4-nitrotoluene, ethylene glycol dinitrate, and 2,3-dimethyl-2,3-dinitrobutane (DMDNB).[17] DMDNB, a volatile organic compound, is the most commonly used taggant in the United States since it has no wide industrial use, has a high vapor pressure (2.07×10^{-3} Torr at 298 K),[16] and a very low concentration is required for its detection (roughly 0.1% as compared to approximately 0.5% of 2- or 4-dinitrotoluene).[18] While gas-phase detection of DMDNB is well established, difficulty would be found detecting this taggant within an explosive that is sealed in an airtight container. In this work, we present THz spectroscopy of solid-state DMDNB and investigate the origins of its characteristic THz spectrum[1] that could be used to detect and identify the substance.

Recording experimental THz spectra of such compounds is only part of the overall investigation, as the rational use of such data in analytical applications requires confident assignments of the observed features to specific atomic motions. Solid-state

Received: March 14, 2012
Revised: May 22, 2012
Published: May 30, 2012

   dx.doi.org/10.1021/jp302487t | J. Phys. Chem. A 2012, 116, 6879−6884

density functional theory (DFT) permits the full THz spectrum of a crystalline substance to be assigned and removes any doubt on the chemical origins of the experimental features that could arise from unintended sources such as atmospheric water hydration or structural polymorphs. Solid-state DFT is also particularly useful for interpreting THz spectra since the typical method of isotopic substitution for spectral elucidation has limited effectiveness in this low-frequency region.[19] While use of standard DFT functionals (B3LYP, PBE0, etc.) and basis sets is often sufficient for the accurate reproduction of experimental data, limitations of such approaches are revealed in molecular crystals that are characterized by weak noncovalent intermolecular forces, specifically London dispersion forces. Typical functionals tend to lack a proper description of these forces and, in most cases, completely ignore such interactions. The consequence of this neglect is that the binding energy between the molecules is underestimated and geometry optimizations yield structures with unreasonable increases in unit cell volume. These physically unrealistic structures then result in inaccurate frequency simulations. This has been addressed here by applying semiempirical dispersion corrections to the DFT energies.[20,21] This combined experimental and computational investigation of the THz spectrum of DMDNB has enabled a complete assignment of the low-frequency vibrations to be made and permits an evaluation of its merits as a THz-active explosives taggant.

2. METHODS

2.1. Sample Preparation. Commercially available DMDNB was obtained from Sigma-Aldrich with 98% purity. Used without further purification, the DMDNB samples were mixed with a spectroscopic grade powdered polytetrafluoroethylene (PTFE) matrix. Dilution of DMDNB with PTFE, which is mostly transparent in the THz region, ensures that the concentration of the sample pellet is within an optimal absorption range. The sample and the matrix were then mechanically pulverized using a stainless-steel ball mill (Dentsply Rinn 3110-3A). This allowed for a homogeneous distribution of the sample through the matrix, reduced the particle size, and thus minimized radiation scattering.[22,23] The mixture was then pressed into a pellet at 2000 psi using a hydraulic press (ICL E-Z Press 12). The resulting sample pellet had a total mass of 0.55 g, thickness of 2.0 mm, diameter of 13.0 mm, and contained 1.7% DMDNB w/w. The blank (reference) pellet was prepared with pure PTFE in a similar manner.

2.2. Time-Domain Terahertz Spectroscopy. The experimental THz spectra were acquired using a pulsed time-domain THz spectrometer based on an amplified femtosecond Ti:Sapphire laser system operating in the near-infrared region. The instrument utilized optical rectification[24,25] and free space electro-optic sampling[24,26] in ZnTe crystals for generation and detection of THz radiation, respectively. A detailed description of the spectrometer along with the experimental setup has been provided elsewhere.[27−29] The sample and blank pellets were both held under vacuum in a variable-temperature cryostat and held at temperatures of 293 K (room temperature) and 78 K (liquid-nitrogen temperature).

Each individual spectrum of the sample (or the blank pellet) consisted of an average of 32 THz waveform scans over a time window of ∼30 ps. These waveforms were then symmetrically zero-padded to a total of 6000 data points before Fourier-transforming into the frequency-domain. Elimination of any THz absorption by the PTFE matrix was accomplished by taking a ratio of the transformed spectrum of a PTFE blank versus the transformed spectrum of a sample pellet. To improve the final signal-to-noise ratio, four blank/sample sets were collected and averaged, yielding the THz spectra ultimately reported here. The THz absorption spectra cover a range of 10 to 90 cm^{-1} with a spectral resolution of approximately 1.0 cm^{-1}.

2.3. Solid-State Density Functional Theory. Density functional theory calculations on solid-state DMDNB were performed using the CRYSTAL09 software package.[30,31] For these computational studies, the B3LYP[32−34] hybrid density functional was utilized in combination with the 6-311G(2d,2p) Gaussian-type basis set.[35−37] The effectiveness of the combination of the B3LYP density functional with the 6-311G(2d,2p) basis set has been demonstrated previously,[38] and only results using this method are reported here. In all DMDNB calculations, a total of 566 902 grid points, defined by a pruned (75,974) DFT integration grid consisting of 75 radial and 974 angular points, has been used (XLGRID program option).[31,39] The total energy convergence was set to $\Delta E < 1 \times 10^{-8}$ hartree for optimizations and $\Delta E < 1 \times 10^{-11}$ hartree for frequency calculations. The truncation tolerances used to control the accuracy of the bielectronic Coulomb and exchange integral series were set to 10^{-10}, 10^{-10}, 10^{-10}, 10^{-10}, and 10^{-20} hartree (TOLINTEG command).[31,39] By sampling and monitoring the total energy convergence as a function of k-point count, the appropriate shrinking factors, that control the accuracy of reciprocal space integration for Fermi energy calculations and density matrix reconstruction, were determined. A factor of 6 has been used for both shrinking factors of reciprocal lattice vectors as defined by the Pack−Monkhorst net[40] and the Gilat net,[41,42] with each containing 112 k-points in the irreducible Brillouin zone.

The unit cell parameters and initial atomic positions used as the basis for structural optimization calculations were obtained from previously reported X-ray diffraction measurements.[43] The crystal structure of DMDNB at 95 K was determined to be triclinic with a space group of $P\bar{1}$(#2) with unit cell dimensions of a = 6.300 Å, b = 6.380 Å, c = 11.851 Å, and α = 100.73°, β = 81.00°, γ = 118.72°. Each unit cell contains two molecules (Z = 2) with one asymmetric molecule (Z' = 1).

Finally, using the optimized DMDNB structures, harmonic normal-mode frequencies and infrared (IR) intensities were calculated. The IR intensity of each mode was calculated from dipole moment derivates ($d\mu/dQ$) based on Born charge tensors, which were determined through numerical evaluations of the polarization differences (Berry phase approach) between the central and the distorted geometries of the unit cell.[31,35,44]

3. RESULTS

3.1. Experimental THz Spectra. Terahertz spectra of DMDNB obtained at 293 and 78 K over a spectral range of 10.0 to 90.0 cm^{-1} are shown in Figure 1. In both cases, absorption features are observed, but the cold spectrum reveals considerably more detail. At room temperature, the THz spectrum consists of two apparent spectral features centered at 38.3 and 49.2 cm^{-1} with an average full-width half-maximum (fwhm) line width of 10.0 cm^{-1} as determined by a Lorentzian peak shape analysis. These peak positions correspond with the previously observed spectrum reported by Zhang, et al.[1] Once the sample is cooled to 78 K, thermally populated vibrational states are decreased, causing line width narrowing. Con-

dx.doi.org/10.1021/jp302487t | J. Phys. Chem. A 2012, 116, 6879−6884

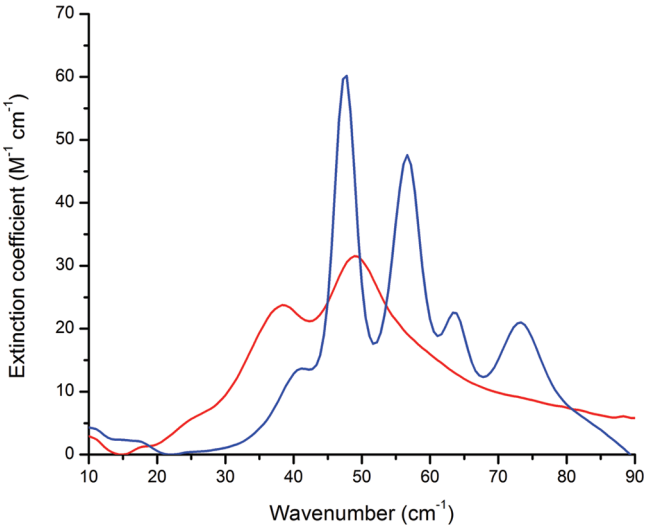

Figure 1. Room temperature (red, 293 K) and cryogenic (blue, 78 K) experimental THz spectra of DMDNB. The experimental spectra are vertically offset slightly, placing the minimum absorbance of each spectrum at zero.

sequently, along with frequency shifting of the originally observed features to higher energy, additional peaks appear that were not resolved in the room-temperature spectrum. At 78 K, the THz spectrum exhibits features with 5.0 cm^{-1} fwhm line widths and frequency centers of 40.1, 47.5, 56.6, 63.9, and 73.6 cm^{-1}.

3.2. Density Functional Theory Analyses. *3.2.1. Calculations with Fixed Lattice Dimensions. 3.2.1.1. DMDNB Structure Simulations.* The crystalline structure of DMDNB used in this work was originally studied as part of an investigation of the structures and properties of substituted 1,2-dinitroethanes.[43] The measured crystal structure from X-ray diffraction experiments shows a unit cell that is composed of two molecules ($Z = 2$) related to each other by inversion, with one in the asymmetrical unit ($Z' = 1$). No significant short intermolecular contacts are present, which is consistent with there being no opportunities for hydrogen bonding or other strong interactions between the molecules. In Figure 2a, the labeling scheme of the atoms within the DMDNB molecule is presented, while Figure 2b shows the packing arrangement of

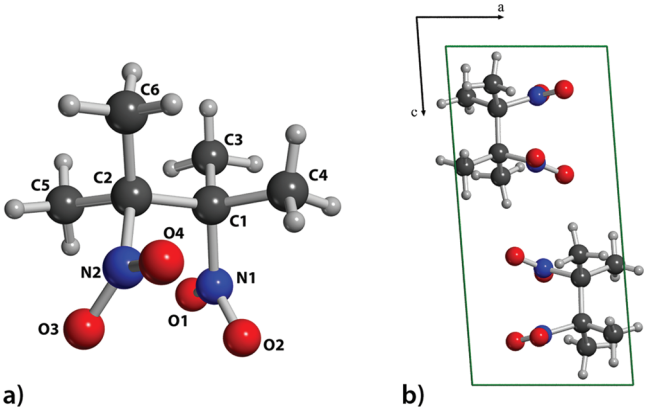

Figure 2. Representation of (a) the labeling scheme of the DMDNB molecule and (b) the crystal packing arrangement of solid-state DMDNB shown along the crystallographic *b*-axis.

the molecules in the crystalline unit cell. Further solid-state investigations of DMDNB showed that the compound does not undergo any polymorphic changes in the temperature range of interest in the current study (78 to 293 K).[43,45] However, additional polymorphs have been reported at higher temperatures, specifically a body-centered cubic polymorph of DMDNB is observed above 388 K.[45]

Using the experimentally obtained 95 K X-ray structure of DMDNB[43] as the starting structure, geometry optimizations were performed using solid-state DFT. In these initial calculations, the atom positions were allowed to optimize within the constraints of the experimentally dictated symmetry and lattice dimensions (fixed unit cell optimization). To evaluate the quality of the geometry reproductions, as compared to the experimentally determined structure, root-mean-squared deviation (rmsd) values of bond lengths, bond angles, and bond dihedral angles were calculated. Only heavy atom positions were used in the evaluation of the rmsds since the positions of the hydrogen atoms is not known to great accuracy in the X-ray diffraction results. The measurements of bond lengths, angles, and dihedrals along with their rmsd values are available in Tables S1, S2, and S3 of the Supporting Information. The bond rmsd value for N−O and C−C bonds was 0.0090 Å, in excellent agreement with the experimentally determined values. Likewise, the rmsds for the optimized bond angles and dihedrals were 0.229° and 0.635°, respectively, correlating well with experiment.

3.2.1.2. DMDNB Frequency Simulations. Using the optimized DMDNB structure, harmonic normal-mode frequencies and IR intensities were calculated. The computed vibrational frequencies and intensities for the IR-active modes are listed and compared to the experimental observations in Table 1. As can be seen in Figure 3b, the simulation using

Table 1. Predicted Frequencies (cm^{-1}), Infrared Intensities ($km\ mol^{-1}$), and Frequency rmsd Values (cm^{-1}) for the DMDNB Infrared-Active Normal Modes in the Experimental Range (10−90 cm^{-1}) with and without Dispersion Corrections As Compared to Experimental Observations

	without dispersion		with dispersion	
exptl frequency	frequency	intensity	frequency	intensity
40.1	40.27	5.90	39.40	3.52
47.5	46.57	13.40	46.94	15.60
56.6	52.71	8.54	58.76	5.70
63.9	65.51	3.09	70.01	3.76
73.6	81.02	5.42	87.96	7.94
rmsd	3.85		7.08	

B3LYP/6-311G(2d,2p) showed a good reproduction of the five experimental spectral features within the investigated range, with a frequency rmsd of 3.9 cm^{-1}. It is important to note that after the simulated intensities were convolved using the empirically measured 5.0 cm^{-1} fwhm line shape, the theoretical intensities were in excellent agreement with the experimental values. No arbitrary scaling of the calculated intensities was needed, and the extinction coefficient units used in Figure 3 correspond directly between experiment and simulation.

The good reproduction of the experimental features allowed for assignment of the peaks to specific vibrational motions. Terahertz spectra of molecular solids are often dominated by external lattice vibrations, but here, the THz spectrum of DMDNB originates largely from internal torsional motions of

dx.doi.org/10.1021/jp302487t | J. Phys. Chem. A 2012, 116, 6879−6884

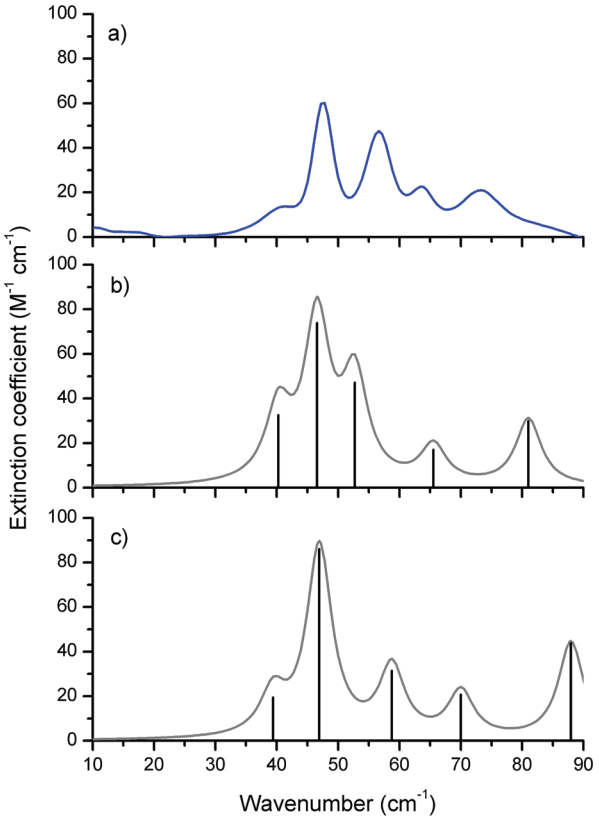

Figure 3. Comparison of (a) the experimental (78 K) and the simulated B3LYP/6-311G(2d,2p) solid-state THz spectra of DMDNB (b) without and (c) with applied dispersion corrections. The solid gray line is a convolved plot of the simulated spectra, using an empirical 5.0 cm^{-1} full-width half-maximum Lorentzian line shape.

the methyl and nitro groups. The first peak (40.1 cm^{-1} in the experimental spectrum) is due to torsion about the C_1-C_2 bond, while both the 63.9 cm^{-1} and 73.6 cm^{-1} spectral features are due to torsions of the methyl and nitro groups. Lattice vibrations do play a role in this spectrum with the second absorption (47.5 cm^{-1}), and most intense recorded, being due to an external vibration consisting of hindered rigid rotations of the individual DMNB molecules about the crystallographic *b*-axis. The third peak (56.6 cm^{-1}) exhibits a more complicated motion and originates from a mixed vibration consisting of components of external molecular rotation and internal torsional motions of the nitro groups.

3.2.2. Fully Relaxed Simulations Using London Dispersion Corrections. As mentioned earlier, there are no particularly strong intermolecular forces binding the DMDNB crystal together, meaning that weak London force interactions play a significant role in the packing of the molecules into their crystalline arrangement. Indeed, when the DMDNB crystal structure was allowed to completely relax during geometry optimizations, with only symmetry restrictions imposed, the calculations yielded structures with physically unreasonable unit cell expansions, exceeding the volume of the 95 K structure by 22.9% and even exceeding the room temperature volume by 16.3%. This expansion upon fully relaxed optimization reveals the limitations of many density functionals and is the reason why fixed unit cell optimizations often provide superior simulations even though they contain some degree of energetic strain from the applied constraints. It is, of course, desirable to allow for completely flexible structural optimizations to be achieved and so calculations were pursued that focused on London force corrected DFT methods.

This unreasonable expansion in volume of the fully optimized structures is due to the lack of inclusion of weak intermolecular interactions (London dispersion forces) within the crystalline environment that play a large role in binding the molecules together and in dictating the crystal packing arrangement. Since standard DFT functionals lack proper description and inclusion of these weak noncovalent intermolecular forces, dispersion corrections need to be applied in fully relaxed structural optimizations and subsequent frequency simulations. A semiempirical correction where the functionals have been augmented to include damped dispersion interactions with factors including dispersion coefficients, van der Waal radii, and a global scaling factor (s_6), has been proposed by Grimme[20] and further modified by Civalleri[21] to be applicable to molecular crystals.

The impact of dispersion corrections was tested as a function of s_6 value and evaluated based on its effect on the unit cell volume (Figure 4) and dimensions (Supporting Information,

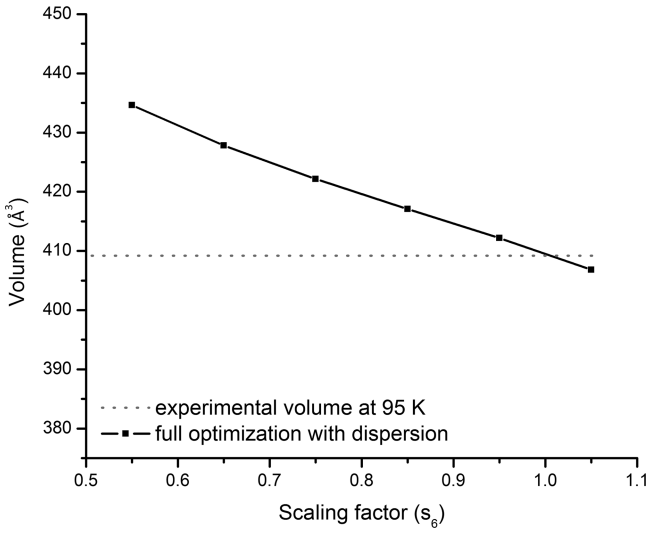

Figure 4. Effect of dispersion corrections in the simulation of the unit cell volume of crystalline DMDNB. An s_6 = 0.00 yields a volume of 503.013 Å^3.

Figures S1 and S2) of the fully optimized DMDNB unit cell. It can be seen that a complete neglect of the dispersion correction, s_6 = 0.00, results in a structure that has an unreasonable increase in unit cell volume. In contrast, utilizing the s_6 value of 1.05 as recommended for calculations using the B3LYP functional,[21] yields a structure close to the experimental one with a volume of 406.797 Å^3 (~0.6% decrease in volume).

This optimized structure using the s_6 = 1.05 dispersion corrections, was then used to calculate the vibrations of the fully relaxed crystal within the same dispersion corrected model. As can be seen in Figure 3c, while the new simulation showed a good reproduction of the first two absorption features, it clearly overestimated the frequency positions of the last three spectral features, with an overall frequency rmsd of 7.08 cm^{-1} (comparing to 3.85 cm^{-1} for the simulation using the fixed-unit-cell optimization). This finding suggests that, while the semiempirical corrections do enable a much more accurate solid-state structure to be attained (compared to full optimizations with no London forces), the improved structure

dx.doi.org/10.1021/jp302487t | J. Phys. Chem. A 2012, 116, 6879−6884

does not guarantee improved vibrational frequencies. In short, correctly identifying the location of the potential energy minimum is different than correctly modeling the curvature of the same energy surface.

All of the significantly shifted vibrations (the three highest frequencies) in the London force corrected spectral simulations have large contributions from nitro group torsional motions. It could be that the London force corrections are overestimated for the interactions of the $-NO_2$ groups and their surroundings, leading to overestimated vibrational frequencies. This could be indicated in the larger dihedral angle rmsd values seen in the London force corrected simulations where the largest errors are found in the nitro group torsional angles (see Table S3 in Supporting Information). Alternatively, it may be that the calculated harmonic frequencies of the dispersion corrected model are correct, but significant vibrational anharmonicity could exist in the torsional motions of the nitro groups leading to the observed discrepancies in those particular vibrations but not in others.

4. CONCLUSIONS

Terahertz spectra from 10 to 90 cm^{-1} were investigated for room-temperature and liquid-nitrogen-cooled 2,3-dimethyl-2,3-dinitrobutane. At both temperatures, distinct features were observed in the THz spectra, with two peaks measured at 293 K and five peaks at 78 K. Using the experimental cryogenic structure of DMDNB, solid-state DFT structural optimizations and frequency analyses were performed. Both the experimental DMDNB crystal structure and the cold THz spectrum were very well reproduced by the DFT simulations, further showing the utility of solid-state DFT computational methods for the accurate prediction and assignment of the THz spectra of molecular crystals. Much of the THz spectrum was found to originate in internal molecular vibrations rather than the external lattice vibrations that often dominate solid-state THz spectra. The spectral simulations using London force corrected DFT suggest that there may be significant vibrational anharmonicity in the torsional motions of the nitro groups in this frequency region. Terahertz spectroscopy has previously been demonstrated to be an effective technique for the detection and identification of solid-state explosives. Here, we have detailed an investigation of an explosive taggant that also exhibits a unique THz signature and so may be used as an indicator of the presence of an explosive in an otherwise THz-inactive sample. However, since DMDNB by itself is a weak THz absorber, with a peak extinction coefficient of ~30 M^{-1} cm^{-1} at room temperature, this particular taggant could be difficult to detect. The development of strong THz-active taggants for explosives marking would be of great use for future applications of THz spectroscopy in this area.

■ ASSOCIATED CONTENT

Supporting Information

Effect of dispersion corrections in the simulation of the unit cell dimensions of crystalline DMDNB. Calculated solid-state bond lengths, bond angles, and bond dihedral angles of DMDNB. This material is available free of charge via the Internet at http://pubs.acs.org.

■ AUTHOR INFORMATION

Corresponding Author

*E-mail: tmkorter@syr.edu.

Notes

The authors declare no competing financial interest.

■ ACKNOWLEDGMENTS

Funding for this work was provided by a grant from the National Science Foundation CAREER Program (CHE-0847405). E.M.W. would like to thank Syracuse University and the SMART Scholarship Program for financial support.

■ REFERENCES

(1) Chen, J.; Chen, Y.; Zhao, H.; Bastiaans, G. J.; Zhang, X. C. *Opt. Express* **2007**, *15*, 12060.
(2) Leahy-Hoppa, M. R.; Fitch, M. J.; Zheng, X.; Hayden, L. M.; Osiander, R. *Chem. Phys. Lett.* **2007**, *434*, 227.
(3) Shen, Y.; Taday, P. F.; Kemp, M. C. *Proc. SPIE: Int. Soc. Opt. Eng.* **2004**, *5619*, 82.
(4) Schmuttenmaer, C. A. *Chem. Rev.* **2004**, *104*, 1759.
(5) Beard, M. C.; Turner, G. M.; Schmuttenmaer, C. A. *J. Phys. Chem. B* **2002**, *106*, 7146.
(6) Plusquellic, D. F.; Korter, T. M.; Fraser, G. T.; Lavrich, R. J.; Benck, E. C.; Bucher, C. R.; Hight Walker, A. R.; Domenech, J. L. *Int. J. High Speed Electron. Syst.* **2003**, *13*, 1287.
(7) Strachan, C. J.; Taday, P. F.; Newnham, D. A.; Gordon, K. C.; Zeitler, J. A.; Pepper, M.; Rades, T. *J. Pharm. Sci.* **2005**, *94*, 837.
(8) Allis, D. G.; Fedor, A. M.; Korter, T. M.; Bjarnason, J. E.; Brown, E. R. *Chem. Phys. Lett.* **2007**, *440*, 203.
(9) Li, R.; Zeitler, J. A.; Tomerini, D.; Parrott, E. P. J.; Gladden, L. F.; Day, G. M. *Phys. Chem. Chem. Phys.* **2010**, *12*, 5329.
(10) Siegrist, K.; Bucher, C. R.; Mandelbaum, I.; Hight Walker, A. R.; Balu, R.; Gregurick, S. K.; Plusquellic, D. F. *J. Am. Chem. Soc.* **2006**, *128*, 5764.
(11) Williams, M. R. C.; True, A. B.; Izmaylov, A. F.; French, T. A.; Schroeck, K.; Schmuttenmaer, C. A. *Phys. Chem. Chem. Phys.* **2011**, *13*, 11719.
(12) Jepsen, P. U.; Clark, S. J. *Chem. Phys. Lett.* **2007**, *442*, 275.
(13) Witko, E. M.; Buchanan, W. D.; Korter, T. M. *J. Phys. Chem. A* **2011**, *115*, 12410.
(14) *Convention of the Marking of Plastic Explosives for the Purpose of Detection*; International Civil Aviation Organization: Montreal, Canada, 1991.
(15) *Public Law 104−132: Antiterrorism and Effective Death Penalty Act of 1996*; US Government: Washington DC, 1996.
(16) Paine, M. R. L.; Kirk, B. B.; Ellis-Steinborner, S.; Blanksby, S. J. *Rapid Commun. Mass Spectrom.* **2009**, *23*, 2867.
(17) Munro, W. A.; Paul Thomas, C. L.; Langford, M. L. *Anal. Chim. Acta* **1998**, *374*, 253.
(18) Perr, J. M.; Furton, K. G.; Almirall, J. R. *J. Sep. Sci.* **2005**, *28*, 177.
(19) King, M. D.; Buchanan, W. D.; Korter, T. M. *J. Phys. Chem. A* **2010**, *114*, 9570.
(20) Grimme, S. *J. Comput. Chem.* **2006**, *27*, 1787.
(21) Civalleri, B.; Zicovich-Wilson, C. M.; Valenzano, L.; Ugliengo, P. *CrystEngComm* **2008**, *10*, 405.
(22) Holden, J. R.; Dickinson, C. W. *J. Phys. Chem.* **1975**, *79*, 249.
(23) Lowry, T. M.; Hemmings, F. C. *J. Soc. Chem. Ind., London* **1920**, *39*, 101.
(24) Nahata, A.; Weling, A. S.; Heinz, T. F. *Appl. Phys. Lett.* **1996**, *69*, 2321.
(25) Rice, A.; Jin, Y.; Ma, X. F.; Zhang, X. C.; Bliss, D.; Larkin, J.; Alexander, M. *Appl. Phys. Lett.* **1994**, *64*, 1324.
(26) Wu, Q.; Litz, M.; Zhang, X. C. *Appl. Phys. Lett.* **1996**, *68*, 2924.
(27) Hakey, P. M.; Allis, D. G.; Hudson, M. R.; Ouellette, W.; Korter, T. M. *ChemPhysChem* **2009**, *10*, 2434.
(28) Hakey, P. M.; Allis, D. G.; Ouellette, W.; Korter, T. M. *J. Phys. Chem. A* **2009**, *113*, 5119.
(29) Hakey, P. M.; Hudson, M. R.; Allis, D. G.; Ouellette, W.; Korter, T. M. *J. Phys. Chem. A* **2009**, *113*, 13013.
(30) Dovesi, R.; Orlando, R.; Civalleri, B.; Roetti, C.; Saunders, V. R.; Zicovich-Wilson, C. M. *Z. Kristallogr.* **2005**, *220*, 571.

(31) Dovesi, R.; Saunders, V. R.; Roetti, C.; Orlando, R.; Zicovich-Wilson, C. M.; Pascale, F.; Civalleri, B.; Doll, K.; Harrison, N. M.; Bush, I. J.; D'Arco, P.; Llunell, M. *CRYSTAL09 User's Manual*; University of Torino: Torino, Italy, 2010.
(32) Becke, A. D. *J. Chem. Phys.* **1993**, *98*, 5648.
(33) Lee, C.; Yang, W.; Parr, R. G. *Phys. Rev. B* **1988**, *37*, 785.
(34) Parr, R. G.; Yang, W. *Density-Functional Theory of Atoms and Molecules*; Oxford University Press, New York, 1989.
(35) Krishnan, R.; Binkley, J. S.; Seeger, R.; Pople, J. A. *J. Chem. Phys.* **1980**, *72*, 650.
(36) Ditchfield, R.; Hehre, W. J.; Pople, J. A. *J. Chem. Phys.* **1971**, *54*, 724.
(37) Hehre, W. J.; Ditchfield, R.; Pople, J. A. *J. Chem. Phys.* **1972**, *56*, 2257.
(38) King, M. D.; Korter, T. M. *J. Phys. Chem. A* **2010**, *114*, 7127.
(39) Pascale, F.; Zicovich-Wilson, C. M.; Gejo, F. L.; Civalleri, B.; Orlando, R.; Dovesi, R. *J. Comput. Chem.* **2004**, *25*, 888.
(40) Monkhorst, H. J.; Pack, J. D. *Phys. Rev. B* **1976**, *13*, 5188.
(41) Gilat, G. *J. Comput. Phys.* **1972**, *10*, 432.
(42) Gilat, G.; Raubenheimer, L. J. *Phys. Rev.* **1966**, *144*, 390.
(43) Kai, Y.; Knochel, P.; Kwiatkowski, S.; Dunitz, J. D.; Oth, J. F. M.; Seebach, D.; Kalinowski, H. O. *Helv. Chim. Acta* **1982**, *65*, 137.
(44) Dall'Olio, S.; Dovesi, R.; Resta, R. *Phys. Rev. B* **1997**, *56*, 10105.
(45) Nishizaka, T.; Katuragawa, F.; Sawada, K.; Oda, T.; Koide, T. *Chem. Express* **1987**, *2*, 257.